ADVANCED ENERGY MATERIALS
www.advenergymat.de

Materials Views
www.MaterialsViews.com

Recent Progress in Non-Precious Catalysts for Metal-Air Batteries

Ruiguo Cao, Jang-Soo Lee, Meilin Liu, and Jaephil Cho**

Electrical energy storage and conversion is vital to a clean, sustainable, and secure energy future. Among all electrochemical energy storage devices, metal-air batteries have potential to offer the highest energy density, representing the most promising systems for portable (electronics), mobile (electrical vehicles), and stationary (micro-grids) applications. To date, however, many fundamental issues are yet to be overcome to realize this potential. For example, efficient catalysts for oxygen reduction reaction (ORR) and oxygen evolution reaction (OER) at the air-electrode are yet to be developed to significantly reduce the polarization loss in metal-air batteries, which severely hinders the rate capability, energy efficiency, and operational life. In this progress report, a brief overview is first presented of the critical issues relevant to air-electrodes in metal-air batteries. Some recent advancements in the development of non-precious catalysts for ORR in Li-air and Zn-air batteries are then highlighted, including transition metal oxides, low-dimensional carbon-based structures, and other catalysts such as transition-metal macrocycles and metal nitrides. New directions and future perspectives for metal-air batteries are also outlined.

1. Introduction

The dream of electric vehicles (EVs) has a long history, dating back to the 18th century.[1] Transformation of this dream into reality has become more urgent than ever due to the unsustainable consumption of oil by transportation and its unbearable environmental consequences. However, the lack of suitable batteries and fuel cells with sufficiently high energy and power density has severely hindered the broad acceptance of EVs.[2] For example, the existing electric vehicles have limited driving range, due primarily to the low specific energy density of the available Li-ion batteries. To counter this problem, significant efforts have been devoted to the development of metal-air batteries because of their high theoretical energy density.[3–6] For instance, the projected obtainable energy density of a Li-air battery approaches that of gasoline for automotive applications: ~1700 Wh kg^{-1} (considering that the theoretical energy density for a Li-air battery is about ~11 000 Wh kg^{-1}).[5] Even a more conservative estimate would project a much higher (>4 times) energy density for a Li-air battery than the state-of-the-art Li-ion batteries (150~200 Wh kg^{-1} cell).[7] On the other hand, a Zn-air battery has a theoretical specific energy density of ~1090 Wh kg^{-1}, also an attractive power option for EVs.[8,9] Because of their potential to offer high energy density, significant efforts have been devoted to the development of practical metal-air systems for various applications. To date, however, many scientific and technical challenges still remain to realize the potential for practical applications. One of the critical challenges is to create a reversible and efficient O_2-breathing electrode.[10]

Unlike Li-ion batteries that use intercalation compounds of heavy equivalent weight as electrode materials, metal-air batteries use low equivalent weight metal as the negative electrode and porous, light-weight, carbon based materials as the positive cathode, as schematically illustrated in **Figure 1**a. The main promises of metal-air batteries over traditional batteries include high theoretical energy density and low cost. Among all metal-air batteries, Li-air and Zn-air batteries have attracted the most attention. While Li-air and Zn-air batteries have similar air electrode configuration, they may use different electrode, catalyst, and electrolyte materials and thus have very different performance characteristics. The unique advantages of a Zn-air system include low cost and excellent safety while offering reasonably high energy density. In contrast, a Li-air system has much higher theoretical energy density, offering the best potential to meet the most challenging demands for energy storage in many emerging applications. Further, the remarkable advances made in the negative electrodes for Li-ion batteries may be transferable to Li-air batteries. However, the success in the development of commercially viable metal-air batteries depends critically on the creation of efficient and reversible positive electrodes (or the air electrodes).

Dr. R. Cao, J.-S. Lee, Prof. J. Cho
Interdisciplinary School of Green Energy
Ulsan National Institute of Science and Technology (UNIST)
Ulsan, 689–798, Korea
Website: http://jpcho.com
E-mail: jpcho@unist.ac.kr
Prof. M. Liu
School of Materials Science and Engineering
Georgia Institute of Technology
771 Ferst Drive, NW Atlanta
GA 30332-0245, USA
E-mail: meilin.liu@mse.gatech.edu

DOI: 10.1002/aenm.201200013

While all positive electrodes in a variety of metal-air batteries involve oxygen reduction reaction (ORR) during discharge and oxygen evolution reaction (OER) during charge, there are significant differences in the nature of ORR and OER when different electrolyte is used. For a non-aqueous Li-air battery, oxygen reduction is accompanied by the formation of insoluble Li_2O_2 (or LiO_2) at the surface of catalyst, which will accumulate in the pores of the O_2-breathing cathode.[7] The overall reaction in a Li-air battery with a non-aqueous electrolyte can be described as:

$2Li + O_2 \rightarrow Li_2O_2$ ($E^0 = 2.96$ V) or
$4Li + O_2 \rightarrow 2Li_2O$ ($E^0 = 2.91$ V).

For a Li-air battery with basic aqueous electrolyte, in contrast, the cathodic reaction product LiOH is soluble in the electrolyte, avoiding clogging of air cathode during discharge. The reaction can be described as:

$4Li + O_2 + 2H_2O \rightarrow 4LiOH$ ($E^0 = 3.2$ V).

The major advantage of Li-air batteries is that it has the potential to deliver the highest theoretical energy density with relatively high potentials among all kinds of metal-air batteries.[11] For a Zn-air battery, the reactions at the air electrodes are similar to those in an aqueous Li-air battery; oxygen is reduced to hydroxyl ions (or hydroperoxide ions) during discharge. Zinc ions from the anode can combine with hydroxyl ions to form zincate ions ($Zn(OH)_4^{2-}$), which may decompose to produce ZnO. The overall reaction can be described as:

$2Zn + O_2 \rightarrow 2ZnO$ ($E^0 = +1.65$V).

The advantages of Zn-air batteries include low cost, good safety, and relatively high energy density. However, the performance and applicability of the existing Li-air and Zn-air batteries are limited by similar challenges: low power density, sensitivity to contaminants from air (e.g., CO_2), and electrolyte evaporation due to their open cathode structure.

ORR during discharge and OER during charge play a vital role in determining the performance characteristics of metal-air batteries, including charge-discharge rate, capacity retention, energy efficiency, and cycling life. A typical discharge-charge loop is schematically shown in Figure 1b. The overpotentials from both ORR ($\eta_{discharge}$) and OER (η_{charge}) significantly diminish the power output and round-trip efficiency of metal-air batteries. The ORR process in the air electrode of a metal-air battery includes several steps: oxygen diffusion from outer atmosphere to the catalyst surface, oxygen absorption on the catalyst surface, transfer of electrons from the anode to oxygen molecules, weakening and breaking of oxygen bond, and the removal of hydroxyl ion product from the catalyst surface to the electrolyte (for non-aqueous Li-air, solid product is formed). The OER in a metal-air battery during charge involves the reverse process of the ORR. The factors that affect the performance of the air electrode in a metal-air battery include the activity of catalyst, the morphology of catalyst particles, and the architecture of the air cathode. While significant efforts have been devoted to the development of ORR catalysts with high activity for metal-air batteries in the past few decades,[10,12–16] many practical problems and fundamental questions still remain. Many studies demonstrated that the overpotentials for both ORR and OER can be dramatically decreased by the use of catalytic materials in air electrode.[7,14–18] However,

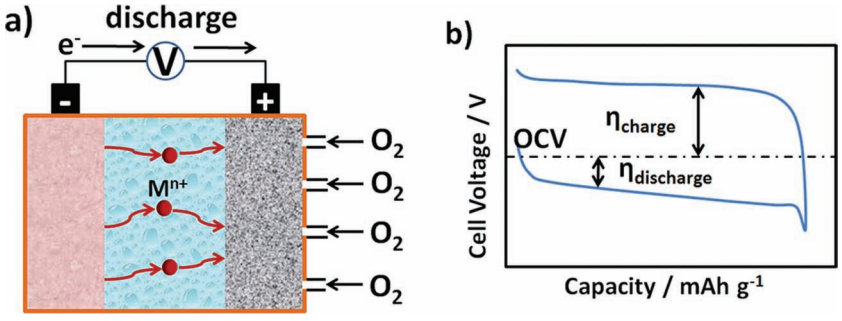

Figure 1. a) A schematic of a metal-air battery composed of a metal as the anode and a porous air electrode as the cathode. b) A typical discharge-charge loop for a metal-air battery.

Meilin Liu is a Regents' Professor of Materials Science and Engineering and Co-Director of the Center for Innovative Fuel Cell and Battery Technologies at Georgia Institute of Technology, Atlanta, Georgia, USA. He received his MS and PhD from University of California at Berkeley. His research interests include preparation, in situ characterization, and multi-scale modeling of materials for energy storage and conversion, aiming at achieving the rational design of novel materials and structures with unique functionalities.

Jaephil Cho is a professor and dean in Interdisciplinary School of Green Energy at UNIST (Korea). He is a director of Converging Research Center for Innovative Battery Technologies (granted by Ministry of Education, Science & Technology of in Korea) and of IT Research Center (granted by Ministry of Knowledge Economy in Korea). His current research is focused mainly on Li-ion and Zn-Air batteries and nanomaterials for energy storage.

Table 1. Summary of catalysts performance in Li-air batteries.

Battery	Catalyst	Capacity	Current density	Reference
Li-air (non-aqueous)	α-MnO_2 nanowire	3000 mAh g^{-1}	70 mA g^{-1}	[12]
Li-air (non-aqueous)	MnO_2/MWNT	1768 mAh g^{-1}	70 mA g^{-1}	[32]
Li-air (non-aqueous)	Ti-doped γ-MnO_2	2200 mAh g^{-1}	0.15 mA cm^{-2}	[33]
Li-air (non-aqueous)	Co_3O_4	4000 mAh g^{-1}	0.02 mA cm^{-2}	[34]
Li-air (non-aqueous)	Graphene	15000 mAh g^{-1}	0.1 mA cm^{-2}	[67]
Li-air (non-aqueous)	Ketjen Black	5813 mAh g^{-1}	0.1 mA cm^{-2}	[42]
Li-air (non-aqueous)	Ketjen Black	1756 mAh g^{-1}	0.01 mA cm^{-2}	[43]
Li-air (solid-state)	N-doped Ketjen Black	1.44 mAh/cell	0.1 mA cm^{-2}	[56]
Li-air (non-aqueous)	N-doped CNTs	866 mAh g^{-1}	75 mA g^{-1}	[57]
Li-air (hybrid)	Graphene	950 mAh g^{-1}	100 mA g^{-1}	[70]
Li-air (non-aqueous)	Carbon fibers	4720 mAh g^{-1}	43 mA g^{-1}	[68]
Li-air (non-aqueous)	Graphene	8705.9 mAh g^{-1}	75 mA g^{-1}	[64]
Li-air (non-aqueous)	Graphene	2332 mAh g^{-1}	50 mA g^{-1}	[65]
Li-air (non-aqueous)	SWCNT/CNF buckypaper	2540 mAh g^{-1}	0.1 mA cm^{-2}	[49]
Li-air (non-aqueous)	Diamond-like carbon	2060 mAh g^{-1}	220 mA g^{-1}	[44]

a recent study suggests that catalysts may be unnecessary for OER during charge in a non-aqueous Li-air battery.[19] To achieve rational design of efficient catalysts for ORR and OER, it is necessary to gain critical insights into the detailed mechanisms of ORR and OER in air electrodes. Even though noble metals and their alloys showed excellent catalytic activity for ORR and OER, they are too expensive to be viable for commercial applications. To be economically competitive, non-precious catalysts must be developed for practical metal-air batteries. To date, several kinds of non-precious catalysts have been explored for use in metal-air batteries, including metal oxides, carbon-based materials, and transition-metal macrocycles. In this progress report, we will focus on the most recent development of a wide variety of non-precious catalysts for ORR in Li-air and Zn-air batteries.

2. Non-Precious Catalysts for Li-Air Batteries

Li-air batteries are considered as the most promising battery system for EV applications because of the much higher theoretical energy density than that of the state-of-the-art Li-ion batteries. However, there is still a long way to go to realize the potential. One of the most important requirements is to develop cheap and efficient catalysts for ORR in air electrodes. For non-aqueous Li-air batteries, the oxygen reduction can be described as follows:[4]

$$O_2 + e^- \rightarrow O_2^-$$

$$O_2^- + Li^+ \rightarrow LiO_2$$

$$2LiO_2 \rightarrow Li_2O_2 + O_2$$

Since the mechanisms of oxygen reduction in a non-aqueous Li-air battery is quite different from those in an aqueous electrolyte, the knowledge from conventional catalysts for fuel cells and aqueous metal-air batteries cannot be straightforwardly applied to non-aqueous Li-air systems. Because solid Li_2O_2 is formed during discharge, porosity of the air electrode is reduced during discharge, which may critically affect battery performance. Non-precious catalysts such as metal oxides and carbon-based catalysts have been extensively investigated and widely used in non-aqueous Li-air batteries to facilitate ORR and OER.[8,10] **Table 1** summarizes the performance of non-precious catalysts in Li-air batteries.

In a Li-air battery with aqueous electrolytes, the ORR is similar to those in an alkaline fuel cell (AFC) or a Zn-air battery. Catalysts developed for AFC and Zn-air batteries can be used in aqueous Li-air batteries. The mechanism of oxygen reduction in aqueous electrolyte has been investigated extensively.[9,20–22] Oxygen molecules can be reduced via a two-electron or a four-electron pathway, producing perhydroxide and hydroxyl ions, respectively. Several types of non-precious catalysts have been studied in aqueous electrolyte, including metal oxides and nitrogen doped carbon materials.

2.1. Metal Oxides

Transition metal oxides such as manganese oxide (MnO_x) and cobalt oxide (CoO_x) have attracted great interests for the applications in metal-air batteries because of their good ORR activity and low cost.[10] To date, MnO_x is the most extensively studied catalyst in non-aqueous Li-air batteries.[23–29] Among all types of MnO_x, α-MnO_2 is considered the most active catalysts in a Li-air battery because its crystal structure facilitates oxygen decomposition and lithium ion coordination.[12,30] The α-MnO_2 structure contains double chains of MnO_6 octahedra with the tunnel structure of (2 × 2) and (1 × 1).[31] The sizes of the 1-dimensional (2 × 2) and (1 × 1) tunnel are ~4.6Å and

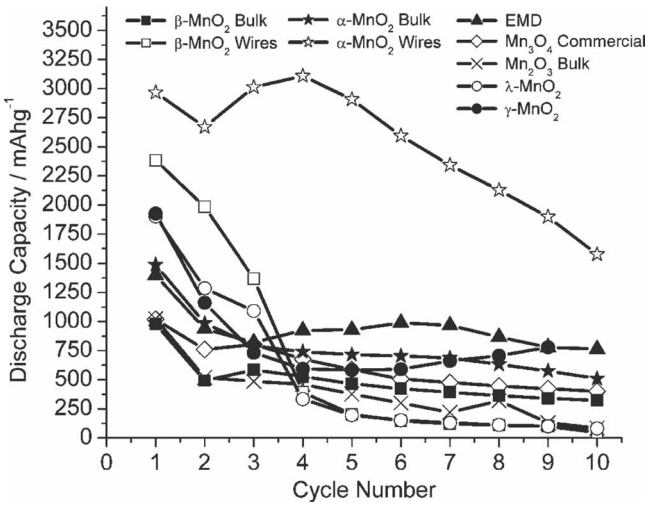

Figure 2. Discharge performance for several types of manganese oxides: α-MnO_2 in bulk and nanowire form, β-MnO_2 in bulk and nanowire form, electrolytic manganese dioxide (EMD), γ-MnO_2, λ-MnO_2, Mn_2O_3 and Mn_3O_4. Cycling rate: 70 mA g^{-1}; O_2 pressure: 1 atm. Reproduced with permission.[12]

~1.89 Å, respectively, which may be helpful to accommodation and absorption of oxygen molecules and lithium ions in the structure. Using α-MnO_2 nanowires as catalyst, Bruce et al. demonstrated a capacity of 3,000 mAh g^{-1} (based on carbon) and 10 cycles with good capacity retention (**Figure 2**).[12] Since then, significant efforts have been devoted to the investigation of the catalytic activity of MnO_x in non-aqueous Li-air batteries. Morphology of MnO_x is an important factor that affects the catalytic activity of MnO_x in Li-air batteries; for example, the MnO_2 nanowire exhibited higher catalytic activity than bulk MnO_2 in both α- and β-phase.[12] Suib and co-workers compared the catalytic activity of α-MnO_2 catalysts with different morphologies in both aqueous and organic electrolytes.[29] Among all catalysts studied, pure nanorod prepared from a solvent-free method displayed the highest ORR catalytic activity in both aqueous and non-aqueous electrolytes (as determined from limiting and exchange current density measurements), which was attributed to its low average oxidation state of manganese, small crystallite size, high surface area, and large pore volume.

To effectively utilize its catalytic activity, MnO_x was supported by a conductive substrate to mitigate its poor electrical conductivity. MnO_x supported by carbon exhibited higher ORR activity than that without conductive substrates in a non-aqueous electrolyte, and consequently improved the capacity of Li-air batteries.[23,32] Another strategy to enhance the catalytic activity of MnO_x is to dope manganese oxides with low-valent elements. By doping with Ni, α- MnO_2 nanorod showed improved catalytic activity over the un-doped counterpart despite decreased pore size and volume.[29] A hollow strutured γ-MnO_2 doped with Ti delivered the highest specific capacity (~2,400 mAh g^{-1}) among all reported results in non-aqueous Li-air batteries, which was even better than γ-MnOOH manganite, the earlier reported highly active catalyst.[33]

Further, other metal oxides such as Fe_xO_y, NiO, CuO and Co_3O_4 also have intrinsic activity for electrochemical oxygen reaction. Bruce and coworkers screened some conventional oxygen electrocatalysts, including mixed metal perovskite $Li_{0.8}Sr_{0.2}MnO_3$, Fe_2O_3, NiO, Fe_3O_4, CuO and $CoFe_2O_4$.[14] The result indicated that the performances of $Li_{0.8}Sr_{0.2}MnO_3$, Fe_2O_3 and NiO were not good in non-aqueous Li-air batteries. Otherwise, among all tested catalysts, Fe_3O_4, CuO, and $CoFe_2O_4$ exhibited the best capacity retention and Co_3O_4 gave the best compromise between the discharge capacity and cyclibility. For lowering charge overpotential, α-MnO_2 nanowires showed the best performance.[30] Recently, a free-standing-type cathode using Co_3O_4 as a catalyst and Ni-foam as a support was developed for rechargeable Li-air battery.[34] This air electrode delivered a capacity of 4,000 mAh g^{-1}(based on Co_3O_4) and exhibited very good durability. The good performance of this free-standing air electrode was attributed to the high catalytic activity of Co_3O_4 and the unique architecture of the substrate.

2.2. Carbon-Based Materials

There are several allotropes of carbon, of which the best known are graphite, diamond, and amorphous carbon. The physical properties of carbon vary widely with the allotropic form. In particular, activated carbon, carbon nanotubes, and graphene have been widely used for energy storage and conversion such as Li-ion batteries and supercapacitors.[35–39] Another emerging area is the use of carbon as metal-free catalysts for chemical processes;[40] the edges and defects may act as catalytic sites for activation of chemical reactions. For oxygen reduction, it has been demonstrated that carbon materials, especially nitrogen doped carbon, exhibited excellent catalytic activity.[10,41] Because of their low cost and high ORR activity, carbon-based materials are promising candidates of metal-free catalysts in air electrodes for Li-air batteries. The factors that influence the ORR activity of different carbon materials include crystal structure, morphology, and defect chemistry.

A carbon-based air electrode was used in a rechargeable non-aqueous Li-air battery by Abraham and coworkers.[13] The rechargeable Li/O_2 cell demonstrated a gravimetric capacity of 1,410 mAh g^{-1}. Since then, much attention has been attracted to the development of more efficient catalysts for Li-air batteries. Different forms of carbon materials were investigated to improve the specific capacity of Li-air batteries. Beattie *et al.* reported that a gravimetric capacity of 5,813 mAh g^{-1} of carbon was achieved at a current density of 0.1 mA cm^{-2} when Ketjen Black was used to prepare the air electrode without any catalyst.[42] Although large gravimetric capacity was reached, the current density is very small. Xiao *et al.* optimized the composition of air electrode using several kinds of carbon materials,[43] reporting a gravimetric capacity of 1,756 mAh g^{-1} for Ketjen Black under optimal conditions, which was contributed to its high mesopore volume. Also, a diamond-like carbon was investigated as a catalyst in a non-aqueous Li-air battery and demonstrated a capacity of 2,318 mAh g^{-1} at a current density of 220 mA g^{-1}.[44]

As discussed earlier, the ORR during charge at the air electrode in a non-aqueous Li-air cell produces insoluble Li_2O_2, which accumulates at the active sites of the air electrode, potentially clogging the pores and thus increasing the resistance to

gas transport through the pores. Further, the catalytic activity of the electrode will be deactivated by the poor conductivity of the insulating Li_2O_2.[45] Accordingly, the pore structures and the architecture of the air electrode are critical to the functioning of non-aqueous Li-air batteries. Significant efforts have been devoted to optimization of air electrode microstructure for non-aqueous Li-air batteries.[6,46–51] Previous study revealed that the discharge capacity of non-aqueous Li-air battery was affected directly by the pore volume of carbon black.[52] The combination of micro-pores on the nanometer scale and macro-pores on the micrometer scale has been studied for non-aqueous Li-air batteries. Yang *et al.* prepared a mesocellular carbon foam composed of bimodal mesopores with diameters at 4.3 and 30.4 nm. The mesoporous carbon outperformed several commercial carbon, offering ~40% higher capacity in non-aqueous Li-air batteries.[53] Tran *et al.* investigated the correlation between the pore structure of gas-diffusion-electrode and the performance in non-aqueous Li-air batteries, and found an almost linear relationship between average pore diameter of carbon catalysts and the capacity of Li-air.[54] Another strategy to maintain proper pore structures during discharge is the modification of catalysts surface to prevent the accumulation of Li_2O_2 on the surface of catalysts. Activated carbon modified with hydrophobic molecules exhibited significantly higher capacity than that without modification.[55]

It is well known that nitrogen doping of carbon materials can enhance the activity for oxygen reduction in aqueous electrolyte.[10] In a solid-state Li-air battery, Kichambare *et al.* demonstrated that nitrogen doped activated carbon with high surface area displayed twice discharge capacity of that for activated carbon without doping.[56] Compared to pristine carbon, nitrogen doped carbon showed a higher cell voltage. In another example, it was reported by Li et al. that nitrogen-doped carbon nanotubes (N-CANTs) exhibited a specific discharge capacity of 866 mAh g^{-1}, which was about 1.5 times higher than carbon nanotubes (CNTs) with a specific discharge capacity of 590 mAh g^{-1}.[57] The good performance of N-CANTs for oxygen reduction in Li-air batteries was clearly related to nitrogen doping of carbon nanotubes, although the detailed mechanism is still under investigation.

Recently, graphene has attracted much attention for a wide range of applications due primarily to its unique electronic structure, good electrical conductivity, high surface area, tunable catalytic activity, and excellent mechanical strength. As a good support, graphene can considerably enhance the catalytic activity of catalysts.[37,58–60] The enhancement is attributed to its physical properties, such as high conductivity and large surface area. Graphene alone can act as catalysts to facilitate some chemical transformation owing to its chemical properties inherent from the sp^2-bonded carbon networks and unique electronic structure.[61–63] To investigate the catalytic activity of graphene for ORR, Li et al. applied graphene nanosheets (GNSs) in air electrode for non-aqueous Li-air batteries.[64] The authors compared the activity between graphene and other materials, including BP-2000 and Vulcan XC-72. The air electrode based on GNSs yielded a high discharge capacity of ~8700 mAh g^{-1} at a current density of 75 mA g^{-1}, compared to ~1900 mAh g^{-1} for BP-2000 and ~1050 mAh g^{-1} for Vulcan XC-72, respectively. The dominant discharge product was Li_2CO_3 and a small amount of Li_2O_2. This result indicated that GNSs can be used as an ideal candidate for Li-air batteries. Sun et al. also compared the catalytic activity of graphene and Vulcan XC-72 for non-aqueous Li-air batteries.[65] Similarly, GNSs outperformed activated carbon during both discharge and charge.

Hierarchical structure is of great importance for many chemical and energy transformation processes. The structural hierarchy plays a vital role in determining the properties and functionalities of electrode and catalyst materials.[66] The hierarchical structure with high surface area is ideally suited for air electrodes since the pores on different length scale may facilitate oxygen diffusion while avoiding pore blockage due to Li_2O_2 deposition during discharge in non-aqueous Li-air batteries. Several strategies were demonstrated to construct a hierarchical structure of air electrode for Li-air batteries. Xiao *et al.* fabricated a novel air electrode consisting of hierarchically porous graphene and investigated its performance in non-aqueous Li-air batteries.[67] A colloidal microemulsion approach was used to construct this hierarchically porous structure with functionalized graphene sheets (GNSs) that contains lattice defects and surface functionalization by hydroxyl, epoxy and carboxyl groups. A bimodal porous structure was formed, which contained three-dimensional, inter-connected pore channels on both the micro- and nanometer length scales (**Figure 3**). An air electrode

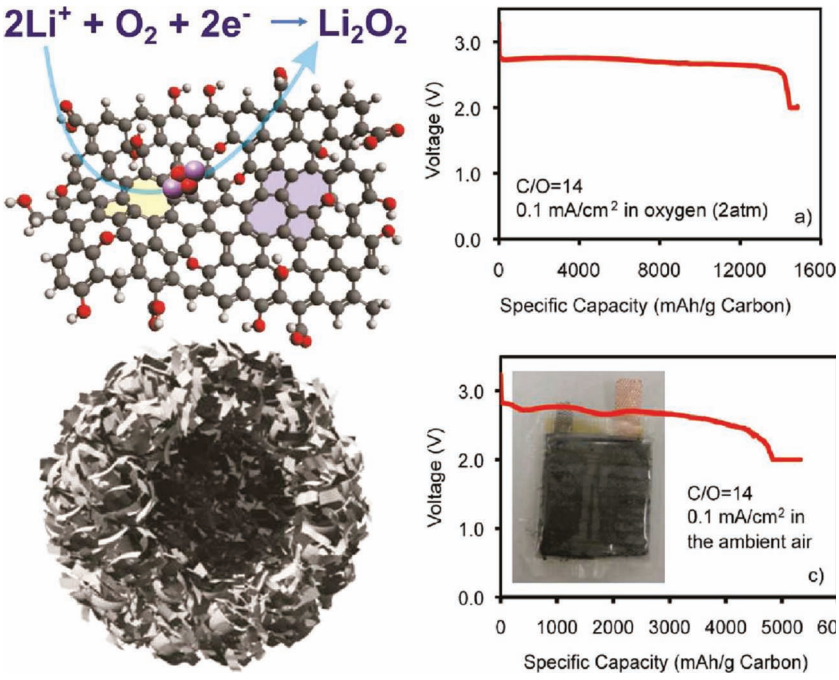

Figure 3. a) A schematic structure of hierarchical graphene sheets. b) Electrochemical performance of hierarchical graphene sheets in a non-aqueous Li-air battery. Reproduced with permission.[67] Copyright 2011, American Chemical Society.

with the unique graphene sheets delivered an extremely high capacity (~15,000 mAh g^{-1}), which is attributed to the unique hierarchical structure. Numerous large tunnels constructed by the macro-pores facilitated continuous oxygen flow into the air electrode while other small "pores" provided ideal multi-phase regions for ORR. DFT calculation also revealed that Li_2O_2 preferred to nucleate and grow near functionalized lattice defects sites on graphene plane.

Another recent approach to fabricate porous carbon air electrode was demonstrated by Shao-horn's group.[68] A new type of binder-free porous carbon electrode configuration was fabricated using a CVD method. Vertically aligned arrays of hollow carbon fibers with diameter on the order of 30 nm were deposited on a porous AAO substrate, which were used as an air electrode in Li-air batteries. The Li-air cells based on this air electrode delivered gravimetric energy densities up to ~2500 Wh $kg_{discharged}^{-1}$ at power densities up to ~100 W $kg_{discharged}^{-1}$, which translated to an energy enhancement ~4 times of that for the state-of-the-art lithium intercalation compounds such as $LiCoO_2$ (~600 W h $kg_{electrode}^{-1}$). The good electrochemical performance was attributed to the more porous structure than other carbon materials, which enhanced utilization efficiency of the available carbon mass and void space for Li_2O_2 deposition during discharge. In addition, the authors studied Li_2O_2 formation and morphological evolution during discharge and its disappearance upon charge, which is helpful to elucidating the charge-discharge mechanism and to the design of highly efficient air electrodes for Li-air batteries.

In a hybrid Li-air battery, the air electrode is immersed in an aqueous electrolyte. Thus, the air-electrode in a hybrid Li-air battery is similar to that in an aqueous Li-air battery.[69] Accordingly, the design for the air electrode should be the same as for an aqueous Li-air battery. However, ORR catalysts for a non-aqueous Li-air battery may have different activity in an aqueous Li-air battery. The edges and defects on the surface of GNSs were reported to be active sites for oxygen reduction in non-aqueous Li-air batteries. Zhou's group demonstrated metal-free graphene sheet showed good performance as a catalyst for the air electrode in a hybrid Li-air battery.[70] GNSs and heat-treated GNSs were used to prepare air electrode for metal-air batteries. The discharge curves for Li-air batteries based on GNSs at a current density of 0.5mA cm^{-2} for 24 h showed a constant voltage of 3.00 V (vs Li/Li^+), compared to 3.05 V and 2.78 V for 20 wt% Pt/CB and acetylene black, respectively, indicating that the metal-free GNSs has good activity for oxygen reduction in a hybrid Li-air battery. The voltage difference between discharge and charge is 0.56 V, which is lower than those reported for other catalysts,[17] indicating that GNSs are effective in lowering the overpotentials of ORR and OER. It was also demonstrated that heat-treatment may enhance the durability of GNSs. Interestingly, an air electrode made from pencil-drawing trace showed good performance in a hybrid Li-air battery.[71] GNSs can be attached on the surface of a ceramic electrolyte by pencil-drawing and was directly tested as the air electrode in a Li-air battery. A discharge capacity of 950 mAh g^{-1} was reached at an end voltage of 2.0 V with a current density of 0.1 A g^{-1}. The cyclability of the air electrode is surprisingly good with little apparent loss after 15 charge-discharge cycles.

2.3. Other Non-Precious Catalysts

In addition to metal oxides and carbon-based materials, other non-precious ORR catalysts such as transition-metal macrocycles (transition-metal porphyrins, transition-metal phthalocyanines, etc.) and metal nitrides also show high activity for oxygen reduction in metal-air batteries. Heat-treatment of transition-metal macrocycles is usually needed to enhance its stability and activity for ORR. Many results revealed that transition-metal ions, coordinated by pyridinic N atom functionalities in heat-treated transition-metal macrocycles, are the active sites for ORR.[20,72,73] However, the detailed coordination structures of the active sites are yet to be identified. Heat-treated FeCu-phthalocyanine (FeCuPc) complexes as the catalyst for oxygen reduction were investigated in non-aqueous Li-air batteries.[74] The Li-air batteries with pyrolyzed FeCuPc catalyst delivered 0.2 V higher discharge voltage at 0.2 mA cm^{-2} than those with pristine carbon. It was shown that the resultant pyrolyzed FeCuPc catalyst not only accelerated the two-electron reduction of oxygen $O_2 + 2Li^+ + 2e \rightarrow Li_2O_2$, but also catalyzed the chemical disproportionation of Li_2O_2 ($2Li_2O_2 \rightarrow 2Li_2O + O_2$). The impedance results indicated that the pyrolyzed FeCuPc catalyst can effectively reduce the apparent activation energy for the discharge of Li-air cells. Ren et al. systematically compared the ORR activity of pyrolyzed CuFePc catalyst supported on Ketjenblack carbon and two other type of carbon materials, SuperP carbon and Ketjenblack carbon, in a Li-air cell with an organic electrolyte.[75] Higher discharge voltage and rate were achieved using pyrolyzed FeCuPc catalyst. The Li-air batteries with pyrolyzed CuFePC catalysts provided higher discharge voltage: ~0.2 V over that with K-carbon and ~0.5 V over that with SP-carbon. The higher cell voltage was attributed to larger density of catalytic site and higher activity of pyrolyzed CuFePc catalysts than pristine carbons.

Metal nitrides are well known as oxygen reduction catalysts in aqueous electrolytes.[9] Recently, a series of nitrogen associated non-precious metal catalyst has been developed for a hybrid Li-air system. For example, titanium nitride as catalyst delivered a cell voltage of 3.8 V at a current density of 0.01 mA cm^{-2} in a hybrid Li-air battery based on acidic electrolyte.[76] A non-aqueous Li-air battery with molybdenum nitride as a catalyst provided a capacity of 1490 mAh g^{-1} and a cell voltage of 3.1 V at the current density of 0.04 mA cm^{-2} demonstrating a higher round-trip efficiency than the cells without molybdenum nitride catalyst.[77]

3. Non-Precious Catalysts for Zn-Air Batteries

Zn-air batteries represent another alternative battery technology for future electric vehicles. The unique advantages of Zn-air over Li-air batteries are low cost and high safety. The porous air electrode for a Zn-air battery is similar to that for an aqueous or a hybrid Li-air battery. In a Zn-air battery, zinc is oxidized on the surface of a porous zinc anode, forming zinc ion which is subsequently transferred to zincate ($Zn(OH)_4^{2-}$) in a potassium hydroxide electrolyte. At the same time, oxygen molecules from the air are reduced to hydroxyl ions through an ORR on the cathode. The theoretical potential for a Zn-air cell is 1.65 V

at 25 °C.[8] The obtainable cell voltage of a Zn-air battery under operation is lower than the theoretical value because of polarization losses. While Pt and its alloy are known efficient catalysts for oxygen reduction, the application of them in Zn-air batteries is limited by their high costs and scarce reserves.[22,78,79] Accordingly, non-precious ORR catalysts have attracted much attention in search for a new generation of Zn-air batteries.[9,73,80–84] In an aqueous electrolyte, oxygen can be reduced by either a direct four-electron pathway with a product of hydroxyl ions or an indirect two-electron pathway with a product of peroxide. The former is more desirable for a Zn-air battery. However, the majority of non-precious ORR catalysts are dominated by an indirect two-electron pathway in alkaline solutions.[21] It is necessary to improve the activity and durability of non-precious catalysts in Zn-air batteries. The non-precious catalysts include metal oxides, nitrogen-doped carbon, transition-metal macrocycles, polymers, and so forth to provide an optimal balance of ORR activity and chemical stability in an alkali electrolyte. The performance of reported non-precious catalysts in Zn-air batteries was summarized in **Table 2**.

3.1. Metal Oxides

Metal oxides, especially manganese oxides, are widely used as catalyst in Zn-air batteries. Since the study of MnO_x for ORR reported by Zoltowski *et al.* in the early 1970s,[85] the electrocatalytic properties of MnO_x toward ORR have been examined as functions of chemical composition, texture, morphology, oxidation state, and crystalline structure.[86–92] For example, the activity of MnO_x with different composition was reported to follow the sequence of $Mn_5O_8 < Mn_3O_4 < Mn_2O_3 < MnOOH$,[86,87] whereas the activity of MnO_2 with different crystal structure to follow the sequence of β- < λ- < γ- < α-MnO_2.[91,92] In addition, the morphological structure, which was related to exposed facets and surface area, was an important factor to affect the catalytic activity of MnO_x toward ORR.[29,91,93,94]

Although significant efforts have been devoted to the enhancement of activity and many studies have been done to show the good activity of MnO_x in alkaline solutions, the detailed mechanism toward ORR of MnO_x is still not very clear due primarily to the complexity of processes and the absence of computational simulation. Several studies revealed that the ORR mechanism of MnO_x involved the reduction and oxidation of surface manganese species and the density of active sites (Mn^{4+}/Mn^{3+}) would dominate the ORR perfomance.[87,89,92,95,96] It was proposed that the materials with distorted structure such as amorphous manganese oxide would exhibit better performance for ORR since it could provide more active sites. In-situ XANES (X-ray absorption near edge structure) results demonstrated that the ORR process involved the reduction of Mn^{4+} to Mn^{3+}, followed by the electron transfer of Mn^{3+} to oxygen.[89]

Since the doping of a low-valent element could enhance the catalytic activity of MnO_x toward ORR, MnO_x doped with a variety of elements (e.g., Ni, Mg and Ca) exhibited higher activity than non-doped materials.[97–100] Roche et al. proposed a four-electron ORR mechanism as follows:[99]

$$MnO_2 + H_2O + e^- \leftrightarrow MnOOH + OH^-$$

$$2MnOOH + O_2 \leftrightarrow (MnOOH)_2 \cdots O_{2,ads}$$

$$(MnOOH)_2 \cdots O_{2,ads} + e^- \rightarrow MnOOH \cdots O_{ads} + OH^- + MnO_2(rds)$$

$$MnOOH \cdots O_{ads} + e^- \leftrightarrow MnO_2 + OH^-$$

In this mechanism, Mn^{4+}/Mn^{3+} species act as oxygen mediator for oxygen reduction. The coexistence of Mn^{4+} and Mn^{3+} species was believed to assist the charge transfer to molecular oxygen and thus facilitate the ORR. The doping of divalent elements such as nickel and magnesium could stabilize the Mn^{4+} and Mn^{3+} species and accordingly enhanced the ORR activity of MnO_x.

Table 2. Summary of catalysts performance in Zn-air batteries.

Catalsyt	ORR Activity	Test Conditions	Battery Performance	Reference
Mn3O4/rGO	Onset: –0.1 V vs Hg/HgO, n = 2~4	0.1 M KOH	120 mW cm^{-2}	[105]
MnO_x/Ketjblack	Onset: –0.05 V vs Hg/HgO	0.1 M KOH	190 mW cm^{-2}	[104]
MnO_x/CNTs	Onset: 0.86 V vs RHE, n = 4	0.1 M KOH	180 mW cm^{-2}	-
Mn_3O_4	0.73 V vs RHE, @ 3 mA/cm^2	0.1 M KOH	-	[106]
$CoMn_2O_4$	–0.08 V vs Ag/AgCl, n = 3.7	0.1 M KOH	335 Wh kg^{-1} @ 10mA	[108]
Co_3O_4/N-rGO	Half-wave: 0.83 V vs RHE, n = 4	0.1 M KOH	-	[110]
Nitrogen-doped carbon nanocapsules	n = 3.96	0.1 M KOH	-	[131]
Graphene-based carbon nitride	n = 4	0.1 M KOH	-	[132]
N-carbon	Onset: 0.035 V vs Ag/AgCl, n = 4	0.1 M KOH	-	[133]
N-CNTs	n = 4	0.1 M KOH	~70 mW cm^{-2}	[134]
B-CNTs	n = 2.5	1 M NaOH	-	[135]
BCN nanotubes	Half-wave: –0.25 V vs SCE, n = 3.7	0.1 M KOH	-	[136]
Fe-phthalocyanine	Half-wave: 0.611 V vs RHE, n = 4	0.1 M KOH	-	[140]

The inherent low conductivity is one of the important drawbacks that limit the activity of MnO_x for ORR. To overcome this limitation, a variety of conducting substrates have been used as current collector for MnO_x catalysts, including different forms of carbons and conductive polymers.[82,101–105] Recently, we have devoted considerable efforts to improving the ORR activity of MnO_x in Zn-air batteries. Our strategy is to tailor the electronic property of MnO_x by crystal structure control to enhance the electrical conductivity using a unique composite design and to improve distribution of active sites through nano-fabrication. One example is to fabricate a composite electrode consisting of MnO_x and graphene.[105] We proposed the introduction of ionic liquid moiety to reduced graphene oxide (rGO) nanosheets to increase not only interaction between graphene sheets and MnO_x nanoparticles, but also ORR catalytic activity based on enhanced utilization of oxygen molecules. This strategy was validated by electrochemical measurements performed on a rotating disk electrode (RDE). The rGO functionalized with ionic liquid moiety exhibited higher limiting current density and more positive onset potential than both graphene oxide (GO) and ionic liquid functionalized graphene oxide (GO-IL). Overloading of manganese oxides (Mn_3O_4) nanoparticles on this functionalized graphene sheet significantly hindered oxygen reduction and even changed the reaction mechanism from a direct four-electron pathway to an indirect two-electron pathway. The enhancement in catalytic activity of MnO_x toward ORR in an alkaline electrolyte is attributed to the increase in electrical conductivity of rGO and the enhanced oxygen molecules affinity by ionic liquid moiety. The result implies a synergic effect between manganese oxide and rGO substrate.

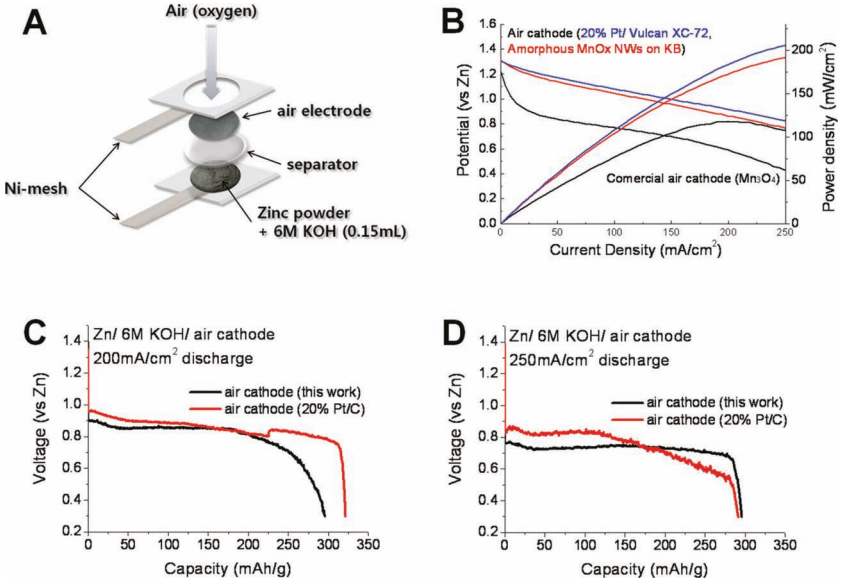

Figure 4. a) A schematic of a Zn-air battery. b) Polarization curves of Zn-air batteries with amorphous MnO_x nanowires, commercial cathode, and commercial Pt catalysts, respectively. c,d) discharge performance of amorphous MnO_x nanowires at current densities of 200 and 250 mA cm^{-2}, respectively. Reproduced with permission.[104] Copyright 2011, American Chemical Society.

Recently, we developed another method to prepare Ketjenblack carbon (KB) supported amorphous manganese oxides nanowires (NWs) via polyol method for Zn-air battery (**Figure 4**).[104] In this approach, low-cost and highly conductive KB was used as substrate to support MnO_x and to promote the growth of amorphous NWs on KB. The unique structure of the composite electrode provides a large number of catalytically active sites for ORR, dramatically increasing the limiting current density and the onset potential in half measurements. The enhanced catalytic activity is resulted from the amorphous NWs structures, which are more accommodative to various geometrical configuration of dioxygen interacting with active metal sites than other crystalline structure. Zn-air batteries with the composite electrode exhibited a peak power density (~190 mW cm^{-2}), which was much better than those with commercial air cathodes (~120 mW cm^{-2}) and was comparable to those with Pt catalyst (~200 mW cm^{-2}).

More recently, we fabricated high power Zn-air batteries using composite electrodes with MnO_x and carbon nanotubes (CNTs) prepared by a facile electroless deposition method. As is shown in **Figure 5**, spontaneously electroless deposition resulted in a good distribution and a well-bonded attachment of MnOx on the surface of CNTs. MnO_x was composed of birnessite crystalline structure, which contained coexistence of Mn^{4+} and Mn^{3+} species and was supposed to deliver very high catalytic activity toward ORR.[99] In half-cell test measurements, the onset potential of MnO_x/CNTs is 0.86 V (vs RHE), with a half-wave potential at 0.75 V. At an ORR current density of 3 mA cm^{-2}, the potential for the MnO_x/CNT composite was 0.75 V, only ~35 mV away from that for the commercial platinum catalyst, which was the best performance comparing with recently summarized data.[106] A high peak power density (~180 mW cm^{-2}) was achieved for the Zn-air cell with the composite cathode, which was comparable to Pt catalyst (~200 mW cm^{-2}) and much higher than commercial air cathode (~117 mW cm^{-2}). The enhancement of catalytic activity is attributed to well-bounded interface between MnO_x and CNTs, which decreases interfacial resistance to facilitate electron transfer from electrode to active sites on the surface of MnO_x particles.

To build rechargeable Zn-air batteries, bifunctional catalysts for both ORR and OER in aqueous electrolyte are necessary. A conventional bifunctional catalyst is usually based on precious metals.[107] To develop a low-cost and high efficient bifunctional electrode is quite challenging owing to the large overpotential for both ORR and OER. A bifunctional catalyst of nanostuctured $Mn_3O_4$was developed by Jaramillo and co-workers.[106] The catalyst design was inspired from a cubane-like $CaMn_4O_x$ active site, the biological catalyst found in the oxygen evolving center in photosystem II in nature. Nanostructured Mn_3O_4 was prepared by a facile electrodeposition method and then calcined at 480 °C. Unlike other MnO_x, the catalytic activity of nanostructured Mn_3O_4 exhibited excellent performance for both ORR and OER, comparable to that of precious metals. The excellent catalytic activity is proposed to be stemmed from

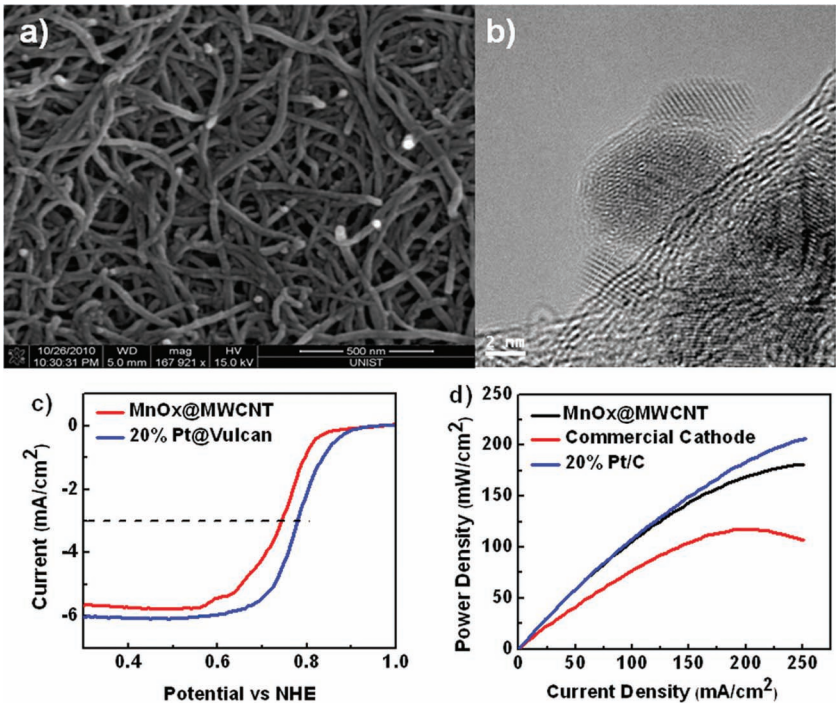

Figure 5. a) SEM and b) TEM images of MnO_x/CNTs composite. c) Linear sweep voltammograms of MnO_x composite and commercial Pt catalyst at a rotation speed of 1600 rpm and a scan rate of 10 mV s^{-1}, in an O_2-saturated 0.1 M KOH solution. d) Polarization curves of Zn-air batteries with MnO_x/CNTs composite, commercial cathode, and commercial Pt catalysts, respectively.

the nanostructured nature of the catalyst. Chen and co-workers developed another facile route to prepare bifunctional catalyst for Zn-air batteries.[108] The nanocrystalline $Co_xMn_{3-x}O_4$ (M = divalent metals) spinels prepared by reduction-recrystallization of amorphous MnO_2 precursors exhibited enhanced catalytic activity towards both ORR and OER. DFT calculation implies the intrinsic electrocatalytic activity for ORR and OER is derived from the different binding energy between oxygen molecule and defect sites.

Co_3O_4 is also a promising candidate of bifunctional ORR/OER catalyst owing to its high electrocatalytic activity and tunable composition.[109] Dai and co-workers developed a low-cost bifunctional catalyst based on a hybrid composite of Co_3O_4 nanocrystal and N-doped graphene.[110] The hybrid composite catalyst (Co_3O_4/N-rGO) outperformed its counterparts, including Co_3O_4, graphene oxide, Co_3O_4/rGO composite and commercial Pt catalyst, toward both ORR and OER. The improvement of catalytic activity is derived from the synergistic effect between catalyst and substrate. The k-edge XANES spectra implied the existence of interfacial Co–O–C and Co–N–C bonds in the Co_3O_4/N-rmGO, which affected the electronic structure of Co_3O_4. Recently, Xu et al. also revealed the importance of tunable electronic structure of Co_3O_4 catalyst.[111] It was found that the ORR catalytic activity of Co_3O_4 catalysts was sensitive to the number and activity of surface-exposed Co^{3+} ions.

Although significant efforts have been devoted to developing metal oxides catalysts for ORR/OER, most catalysts search is based on the method of trial-and-error.[112–116] It is very challenging, but desirable, to find a general principle to guide the material design and synthesis. As a successful example, high active ORR catalysts of Pt-based materials have been developed by following the Sabatier principle.[78,79] Inspired by the Sabatier principle, Shao-horn's group successfully identified an activity descriptor that governs the ORR activity of perovskite in alkaline solutions.[117] After assessing the ORR activity of 15 perovskite-based oxides using a methodology based on a thin-film rotating-disc electrode, it was found that the ORR activity for oxide catalysts primarily correlated to σ*-orbital (e_g) occupation and the extent of B-site transition-metal–oxygen covalency, which served as a secondary activity descriptor. Based on the findings, a volcano trend of the oxide ORR activity was demonstrated and the ORR mechanism on perovskite oxide catalysts was proposed (**Figure 6**). This work provided a general principle to guide how to design perovskite catalysts and improve the ORR activity of future metal oxides catalysts. Soon later, the same group identified the descriptor, occupation of d states with e_g symmetry, for OER over metal oxide catalysts and induced a volcano-shaped activity relationship correlated to the 3d electron with an e_g symmetry of surface transition metal cations in an oxide.[118] Following the volcano plot, a good candidate, $Ba_{0.5}Sr_{0.5}Co_{0.8}Fe_{0.2}O_{3-\delta}$ (BSCF) perovskite, for OER was successfully predicted and prepared. The electrochemical validation of the selected perovskite totally matched the prediction. The catalytic activity of BCSF catalyst led by the design principle outperformed all oxides counterparts and the state-of-the-art iridium oxide catalyst in alkaline media. In a recent

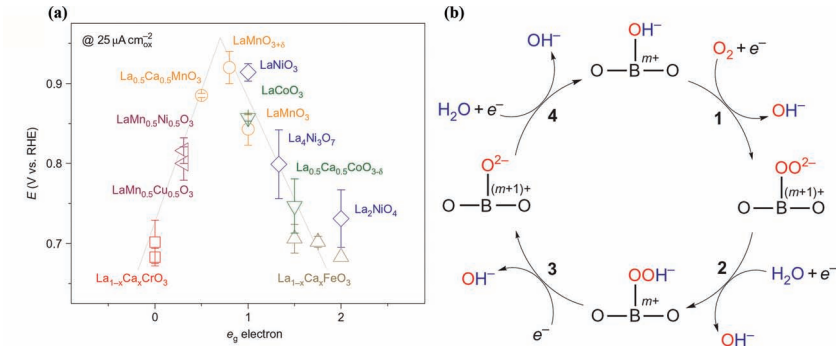

Figure 6. a) Volcano trend of ORR activity for perovskite-based oxides. b) the proposed ORR mechanism on perovskite oxide catalysts. Reproduced with permission.[117] Copyright 2011, Nature Publishing Group.

work, Sr_2CoMoO_6 exhibited relatively higher catalytic activity for ORR than Sr_2FeMoO_6, which is consistent with the volcano-shaped activity trend related to 3d electrons.[119]

3.2. Carbon-Based Materials

Unlike carbon-based catalyst in non-aqueous electrolytes, pristine carbon materials without doping show considerably low catalytic activity for ORR/OER in aqueous solutions. Nitrogen-doping of carbon materials can enhance the catalytic activity for ORR in both acidic and basic electrolyte.[10] Both the contents and lattice structure of nitrogen atoms in carbon materials dominate the catalytic activity toward ORR. Since Dai's group found nitrogen doped carbon nanotubes can activate ORR in an alkaline electrolyte, much efforts have been devoted to the promising metal-free ORR catalysts.[40,41,82,120–127] Learning from the knowledge of nitrogen-doped carbon nanotubes, the same group developed new metal-free catalyst of nitrogen-doped graphene for ORR.[128] The N-doped graphene film possesses remarkable electrocatalytic properties for ORR, similar to that of nitrogen-containing vertically aligned carbon nanotubes, implying the important role of N-doping in carbon materials for ORR. Recent studies demonstrated that carbon nanotubes (either in an aligned or nonaligned form) and graphene, functionalized with certain polyelectrolyte (e.g., poly(diallyldimethylammonium chloride), PDDA), could also act as metal-free electrocatalysts for ORR.[129,130] It indicated that it was unnecessary for ORR activity whether the doped nitrogen atoms were in the carbon lattice. These findings indicate that the intermolecular charge-transfer can serve as a general approach to the cost-effective development of various carbon-based metal-free efficient ORR catalysts.

To develop metal-free catalysts for ORR, several approaches were demonstrated to synthesize nitrogen doped carbon materials. Nitrogen-doped carbon nanotube cups were prepared *via* chemical vapor deposition (CVD) using MeCN, EtOH and ferrocene as precursors, which performed high electrocatalytic activity ORR through combination of two-electron and four-electron pathways.[120] Another simple and efficient route was developed by Shanmugam *et al.* to synthesize nitrogen doped carbon nanocapsules (NCNCs) as a non-noble electrocatalyst for ORR.[131] The method was scalable and reproducible. The NCNCs displayed better performance as a metal-free electrode catalyst for the oxygen reduction in alkaline medium than commercial electrode catalyst with good stability and methanol tolerance.

An effective approach for the fabrication of graphene-based carbon nitride (G–CN) nanosheets was established using a nanocasting technology (**Figure 7**).[132] The G-CN nanosheets contained high nitrogen content, thin thicknesses, high surface areas, and enhanced electrical conductivity. The G–CN nanosheets performed outstanding electrocatalytic activity, long durability, and high selectivity as metal-free catalysts for ORR. Both the electrical conductivity and the content of pyridinic nitrogen atoms are critical to achieve high-performance nitrogen-doped carbon materials for ORR since the combination significantly affects the electron transportation in electrodes and active sites for ORR. A high-surface-area

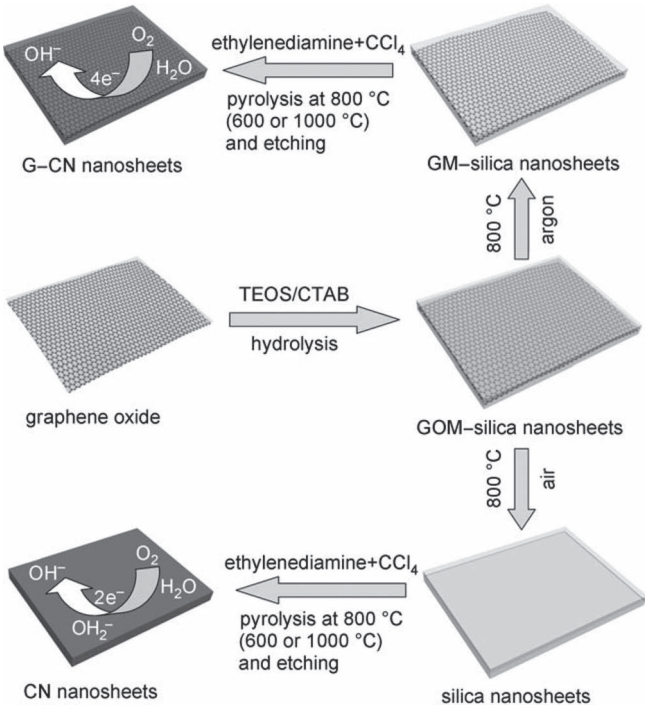

Figure 7. Fabrication of graphene-based carbon nitride (G–CN) and CN nanosheets for ORR. Reproduced with permission.[132]

mesoporous nitrogen-doped carbon material was prepared through the carbonization of ionic liquids and nucleobases by using silica nanoparticles as hard templates.[133] The catalyst contained 12 wt% of nitrogen contents with narrow pore size distribution of *ca.* 12nm diameter. The mesoporous nitrogen-doped carbons exhibited very good electrocatalytic activity for ORR in an alkaline medium. This materials also showed a high methanol tolerance, compare with commercial Pt/C catalyst.In the full-cell tests, nitrogen-doped carbon nanotubes (N-CNTs) derived from ethylenediamine precursors were investigated as air cathode catalyst for Zn-air batteries and exhibited high activity for ORR.[134] A cell power density of ~70 mW cm^{-2} was achieved with an air-cathode catalyst loading of 0.2 mg cm^{-2} and an electrolyte of 6M KOH.

Heat-treatment is a widely-used strategy to improve the catalytic activity and stability of ORR catalysts. A large scale of nitrogen-doped graphene, consisting of both pyridine-like and pyrrole-like nitrogen atoms, was synthesized by heat-treatment of graphene with ammonia.[122] The product annealed under 900 °C exhibited better performance for oxygen reduction than that under 800 and 1000 °C, which contained more pyridine-like nitrogen atoms than others. The electrocatalytic activity and durability of this material were comparable or better than the commercial Pt/C.

Despite nitrogen doping for carbon materials, other elements such as boron and phosphorous doping for carbon materials also can enhance the catalytic activity of carbon materials for ORR. Boron-doped carbon nanotubes (BCNTs) prepared by CVD method exhibited good performance for ORR.[135] The electrocatalytic activity was improved progressively with increasing

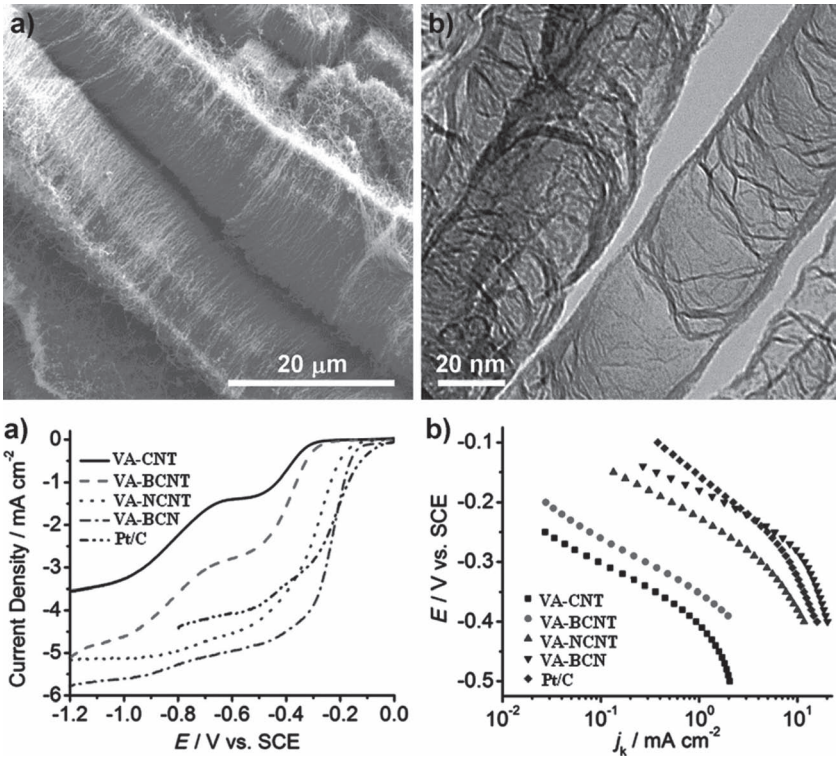

Figure 8. a) SEM and b) TEM images of VA-BCN nanotubes. c,d) electrocatalytic activity of VA-BCN nanotubes in oxygen-saturated 0.1 M KOH electrolyte at a scan rate of 10 mV s^{-1} and a rotation rate of 1000 rpm. Reproduced with permission.[136]

boron content. DFT calculations revealed that electron-deficient boron dopants were positively charged in the BCNT lattice and induced the chemisorptions of oxygen molecules on BCNTs. The electrocatalytic activity of BCNTs for ORR derived from the electron accumulation in the vacant $2p_z$ orbital of boron dopant from the π^* electrons of the conjugated system which then transfer to the chemisorbed oxygen molecules through boron as a bridge. The transferred charge weakened the O-O bonds and, as a result, facilitates the ORR on BCNTs. Carbon nanotubes doped with both boron and nitrogen (BCN nanotubes) can further enhance the catalytic activity toward ORR (**Figure 8**).[136] Comparing to carbon nanotubes doped with nitrogen atoms or boron atoms alone, the BCN nanotubes exhibited higher electrocatalytic activity in an alkaline medium. The better performance stemmed from the synergetic effect of co-doping with boron and nitrogen.

3.3. Other Non-Precious Catalysts

Transition-metal macrocycles, such as transition-metal porphyrins and phthalocyanines, were widely used as electrochemical catalysts for ORR in fuel cells and metal-air batteries.[9,20,21,41] The main disadvantage of transition-metal macrocycles is the poor durability and unclear active sites. Several strategies have been developed to enhance the activity and stability of macrocyclic catalysts for ORR. One of successful example is to construct a face-to-face structure of cobalt porphyrins.[137–139] The dicobalt face-to-face porphyrins can improve the activity and stability for oxygen reduction. Recently, Li *et al.* designed and synthesized a new highly durable iron phthalocyanine based non-precious ORR catalyst (Fe-SPc) in alkaline medium.[140] The design of Fe-SPc catalyst was inspired by the structure of naturally occurring oxygen activation catalysts, enzymes with unique atomic structure and surface properties. By tuning the steric and electronic structure of catalysts, ORR stability of the Fe-SPc was significantly improved after modified by functional groups. Despite organic functionalization, pyrolysis is a widely used strategy to enhance the stability of transition-metal macrocycles. The pyrolysis temperature is an important factor to affect the stability and activity of the complex catalysts. It was found that pyrolyzed tetra methoxyphenyl porphyrin cobalt complex (CoTMPP) at 410 °C had higher catalytic activities than the catalyst pyrolyzed at 800 °C.[141] The pyrolyzed CoTMPP catalysts were tested as ORR catalysts in air electrode for a Zn-air battery. A current density of ~120 mA cm^{-2} was reached at 1 V cell voltage.

A non-precious catalyst based on nitrogen chelated iron or cobalt (FeCo-EDA) has been noted to be a potential ORR catalyst for Zn-air batteries.[142] The electrochemical stability of non-precious FeCo-EDA and commercial Pt/C cathode catalysts were compared in air electrodes for Zn-air batteries. The FeCo-EDA catalyst outperformed commercial Pt/C catalyst in both stability and mass activity. A higher peak power density (~232 mW cm^{-2}) was achieved using FeCo-EDA, comparing to a power density (~196 mW cm^{-2}) for commercial Pt/C.

A variety of conductive polymers, such as polyaniline (PANI), polypyrrole (PPy) and polythiophen (PTh), have been found to have electrocatalytic activity for oxygen reduction.[143] Recently, a type of intrinsically conductive polymer (ICP), poly(3,4-ethylenedioxythiophene) (PEDOT), was found to have surprisingly high activity for oxygen reduction in alkaline medium.[144] An air electrode was fabricated by coating a PEDOT electroactive layer onto one side of a hydrophobic, porous membrane (Goretex), involving plasma polymerization of a binding layer to the polytetrafluoroethylene (PTFE) membrane, followed by polymerization of the 3,4-ethylenedioxythiophene monomer to form the PEDOT conducting polymer. The Goretex/PEDOT electrode was tested as an air electrode at various pH levels. As a result, the Goretex/PEDOT electrode provided substantial oxygen reduction current densities at all of the pH conditions studied. For a full cell test, a Zn-air battery was constructed based on this PEDOT air-electrode and a 1 M KOH electrolyte, which provided an open-circuit voltage of 1.44 V. Based on a 48 h continuous test, the PEDOT air electrode conducted a better performance than a Pt/Goretex air electrode under same test conditions.

Table 3. Characteristic summary of non-precious catalysts in metal-air batteries.

Catalsyt	Activity	Stability	Cost
Metal oxides	high	Moderate	moderate
Carbonaceous materials	moderate	good	low
Transition metal complexes	good	good	high

4. Conclusion and Outlook

Metal-air batteries are perceived to the next generation battery technology because they have potential to meet the ever-increasing demands of electrical energy storage for many emerging applications such as electric vehicles and smart grids. To realize the potential, it is vital to achieve rational design of highly active non-precious catalysts with good stability for oxygen reduction in metal-air batteries. While the detailed mechanism of ORR in metal-air batteries is still unclear, several types of non-precious catalysts have showed very promising catalytic activity and stability, including metal oxides, carbonaceous materials, and transition-metal macrocycles. Among them, metal oxides are the most widely studied non-precious catalysts in Li-air and Zn-air batteries. In particular, MnO_x has been intensely investigated for ORR in both Li-air and Zn-air batteries. The combination of crystalline structure and morphology determines the activity for ORR. For carbonaceous materials, proper doping plays a critical role in tailoring the activity for ORR; the morphology and pore size are important as well. In addition, transition metal complexes are an important alternative catalyst for ORR. The molecular structure of transition metal complexes should be carefully designed. **Table 3** summarizes the characteristics of major ORR catalysts studied for Li-air and Zn-air batteries.

While many non-precious catalysts have showed promises for metal-air batteries, difficulties still remain to develop a practical metal-air battery with performance better than the existing Li-ion batteries. Based on our current understanding of the existing catalysts (**Figure 9**), we believe that the following research directions are important to the development of highly-efficient non-precious catalysts for metal-air batteries.

1) Since both ORR and OER in an air electrode involve multi-phases (liquid, solid, gas), rational design of the interfaces is critical to optimize the catalytic activity. Further, since the solubility of oxygen in liquid electrolytes is relatively low, it is necessary to control hydrophobicity and porosity of the electrodes and catalysts to avoid flooding of the active sites.
2) The electrode or catalyst materials should have highly electrical conductivity for efficient current collection. Insufficient electrical conductivity of catalysts must be mitigated by the use of highly-conductive current collectors/substrates. Further, the contact between catalysts and current collectors must be adequate to ensure easy electron transfer across the interfaces.
3) Catalytic activity of catalysts may be influenced critically by the geometric and the electronic structures of catalysts, which correlate with the binding affinity of oxygen on the surface of active sites. Computational quantum chemistry may be helpful in predicting the catalytic activity and design of catalyst materials. Further, surface nanostructure and local morphology of catalysts may affect the orientation and binding energy of oxygen adsorbed to active sites.
4) Nature-inspired structures may be useful to development of oxygen-breathing air electrode system. For example, respiratory organs such as highly porous fish's gill and human being's lung consume oxygen effectively in liquid and gas phase, as schematically illustrated in **Figure 10**. The structural features of these biological systems, such as large specific surface area and high porosity, may give us some clues about how to design good air electrode structures. The bio-inspired structures have potential to offer excellent air electrode structures for metal-air batteries.

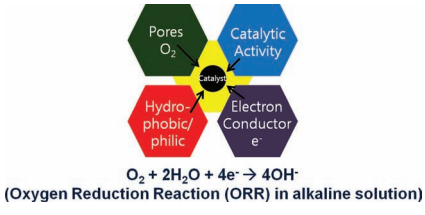

Figure 9. Factors that may affect the rate of oxygen reduction reaction (ORR) in an alkaline solution.

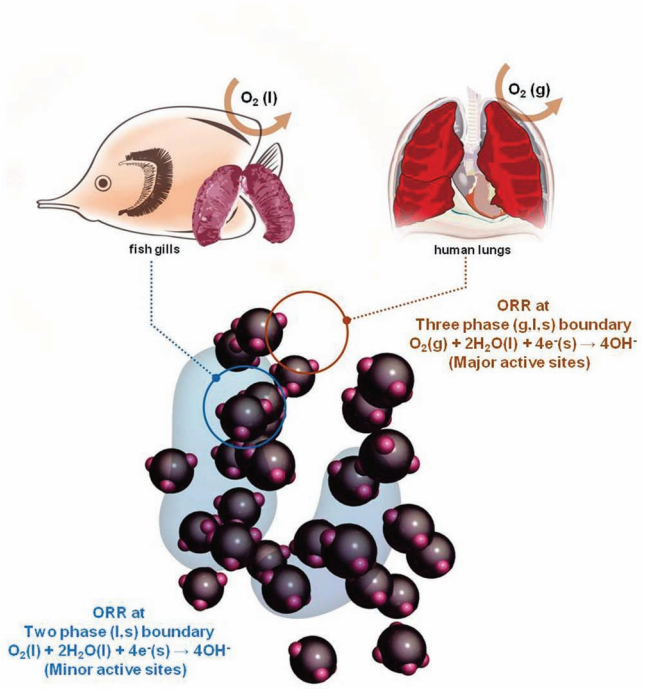

Figure 10. A schematic illustration of biological respiratory organs, such as highly porous fish's gill and human being's lung, and ORR catalysts in an air electrode.

Acknowledgements

This work was supported by the World Class University (WCU) program supported by National Research Foundation (NRF) and the Ministry of Education, Science and Technology (MEST) of Korea. Also, this research was supported by the MKE (The Ministry of Knowledge Economy), Korea, under the ITRC (Information Technology Research Center) support program supervised by the NIPA (National IT Industry Promotion Agency) (NIPA-2011-C1090-1100-0002).

Received: January 5, 2012
Revised: February 29, 2012
Published online: June 15, 2012

[1] O. Park, Y. Cho, S. Lee, H. Yoo, H.-K. Song, J. Cho, *Energy Environ. Sci.* **2011**, *40*, 1621.
[2] F. T. Wagner, B. Lakshmanan, M. F. Mathias, *J. Phys. Chem. Lett.* **2010**, *1*, 2204.
[3] P. G. Bruce, L. J. Hardwick, K. M. Abraham, *MRS Bull.* **2011**, *36*, 7.
[4] P. G. Bruce, S. A. Freunberger, L. J. Hardwick, J.-M. Tarascon, *Nat. Mater.* **2012**, *11*, 19.
[5] G. Girishkumar, B. McCloskey, A. C. Luntz, S. Swanson, W. Wilcke, *J. Phys. Chem. Lett.* **2010**, *1*, 2193.
[6] A. Kraytsberg, Y. Ein-Eli, *J. Power Sources* **2011**, *196*, 886.
[7] Y.-C. Lu, H. A. Gasteiger, M. C. Parent, V. Chiloyan, Y. Shao-Horn, *Electrochem. Solid-State Lett.* **2010**, *13*, A69.
[8] J.-S. Lee, S. T. Kim, R. Cao, N.-S. Choi, M. Liu, K. T. Lee, J. Cho, *Adv. Energy Mater.* **2011**, *1*, 34.
[9] V. Neburchilov, H. Wang, J. J. Martin, W. Qu, *J. Power Sources* **2010**, *195*, 1271.
[10] M.-K. Song, S. Park, F. M. Alamgir, J. Cho, M. Liu, *Mater. Sci. Engineering R* **2011**, *72*, 203.
[11] F. Cheng, J. Chen, *Chem. Soc. Rev.* **2012**, *41*, 2172.
[12] A. Debart, A. J. Paterson, J. Bao, P. G. Bruce, *Angew. Chem. Int. Ed.* **2008**, *47*, 4521.
[13] K. M. Abraham, Z. Jiang, *J. Electrochem. Soc.* **1996**, *143*, 1.
[14] A. Débart, J. Bao, G. Armstrong, P. G. Bruce, *J. Power Sources* **2007**, *174*, 1177.
[15] T. Ogasawara, A. Débart, M. Holzapfel, P. Novák, P. G. Bruce, *J. Am. Chem. Soc.* **2006**, *128*, 1390.
[16] Y. C. Lu, H. A. Gasteiger, Y. Shao-Horn, *J. Am. Chem. Soc.* **2011**, *133*, 19048.
[17] Y.-C. Lu, Z. Xu, H. A. Gasteiger, S. Chen, K. Hamad-Schifferli, Y. Shao-Horn, *J. Am. Chem. Soc.* **2010**, *132*, 12170.
[18] Y.-C. Lu, D. G. Kwabi, K. P. C. Yao, J. R. Harding, J. Zhou, L. Zuin, Y. Shao-Horn, *Energy Environ. Sci.* **2011**, *4*, 2999.
[19] B. D. McCloskey, R. Scheffler, A. Speidel, D. S. Bethune, R. M. Shelby, A. C. Luntz, *J. Am. Chem. Soc.* **2011**, *133*, 18038.
[20] C. Bezerra, L. Zhang, K. Lee, H. Liu, A. Marques, E. Marques, H. Wang, J. Zhang, *Electrochim. Acta* **2008**, *53*, 4937.
[21] Z. Chen, D. Higgins, A. Yu, L. Zhang, J. Zhang, *Energy Environ. Sci.* **2011**, *4*, 3167.
[22] Y. Bing, H. Liu, L. Zhang, D. Ghosh, J. Zhang, *Chem. Soc. Rev.* **2010**, *39*, 2184.
[23] H. Cheng, K. Scott, *J. Power Sources* **2010**, *195*, 1370.
[24] D. Zhang, Z. Fu, Z. Wei, T. Huang, A. Yu, *J. Electrochem. Soc.* **2010**, *157*, A362.
[25] R. S. Kalubarme, M. S. Cho, K. S. Yun, T. S. Kim, C. J. Park, *Nanotechnology* **2011**, 22.
[26] A. K. Thapa, T. Ishihara, *J. Power Sources* **2011**, *196*, 7016.
[27] S. Ida, A. K. Thapa, Y. Hidaka, Y. Okamoto, M. Matsuka, H. Hagiwara, T. Ishihara, *J. Power Sources* **2012**, *203*, 159.
[28] G. Q. Zhang, J. P. Zheng, R. Liang, C. Zhang, B. Wang, M. Au, M. Hendrickson, E. J. Plichta, *J. Electrochem. Soc.* **2011**, *158*, A822.
[29] E. M. Benbow, S. P. Kelly, L. Zhao, J. W. Reutenauer, S. L. Suib, *J. Phys. Chem. C* **2011**, *115*, 22009.
[30] V. Giordani, S. A. Freunberger, P. G. Bruce, J. M. Tarascon, D. Larcher, *Electrochem. Solid-State Lett.* **2010**, *13*, A180.
[31] S. Devaraj, N. Munichandraiah, *J. Phys. Chem. C* **2008**, *112*, 4406.
[32] J. Li, N. Wang, Y. Zhao, Y. Ding, L. Guan, *Electrochem. Commun.* **2011**, *13*, 698.
[33] V. M. B. Crisostomo, J. K. Ngala, S. Alia, A. Dobley, C. Morein, C.-H. Chen, X. Shen, S. L. Suib, *Chem. Mater.* **2007**, *19*, 1832.
[34] Y. Cui, Z. Wen, Y. Liu, *Energy Environ. Sci.* **2011**, *4*, 4727.
[35] D. S. Su, R. Schlogl, *ChemSusChem* **2010**, *3*, 136.
[36] G. Wang, L. Zhang, J. Zhang, *Chem. Soc. Rev.* **2012**, *41*, 797.
[37] X. Huang, X. Qi, F. Boey, H. Zhang, *Chem. Soc. Rev.* **2012**, *41*, 666.
[38] L. L. Zhang, X. S. Zhao, *Chem. Soc. Rev.* **2009**, *38*, 2520.
[39] C. Liu, F. Li, L.-P. Ma, H.-M. Cheng, *Adv. Mater.* **2010**, *22*, E28.
[40] D. S. Su, J. Zhang, B. Frank, A. Thomas, X. Wang, J. Paraknowitsch, R. Schlogl, *ChemSusChem* **2010**, *3*, 169.
[41] G. Liu, X. Li, J.-W. Lee, B. N. Popov, *Catal. Sci. Technol.* **2011**, *1*, 207.
[42] S. D. Beattie, D. M. Manolescu, S. L. Blair, *J. Electrochem. Soc.* **2009**, *156*, A44.
[43] J. Xiao, D. Wang, W. Xu, D. Wang, R. E. Williford, J. Liu, J.-G. Zhang, *J. Electrochem. Soc.* **2010**, *157*, A487.
[44] Y. Yang, Q. Sun, Y.-S. Li, H. Li, Z.-W. Fu, *J. Electrochem. Soc.* **2011**, *158*, B1211.
[45] P. Albertus, G. Girishkumar, B. McCloskey, R. S. Sanchez-Carrera, B. Kozinsky, J. Christensen, A. C. Luntz, *J. Electrochem. Soc.* **2011**, *158*, A343.
[46] T. Kuboki, T. Okuyama, T. Ohsaki, N. Takami, *J. Power Sources* **2005**, *146*, 766.
[47] J. Xiao, D. Wang, W. Xu, D. Wang, R. E. Williford, J. Liu, J.-G. Zhang, *J. Electrochem. Soc.* **2010**, *157*, A487.
[48] M. Mirzaeian, P. J. Hall, *Electrochim. Acta* **2009**, *54*, 7444.
[49] G. Q. Zhang, J. P. Zheng, R. Liang, C. Zhang, B. Wang, M. Hendrickson, E. J. Plichta, *J. Electrochem. Soc.* **2010**, *157*, A953.
[50] C.-J. Lan, Y.-F. Chi, T.-S. Chin, *ECS Transactions* **2008**, *3*, 51.
[51] S. R. Younesi, S. Urbonaite, F. Björefors, K. Edström, *J. Power Sources* **2011**, *196*, 9835.
[52] J. Read, *J. Electrochem. Soc.* **2002**, *149*, A1190.
[53] X.-h. Yang, P. He, Y.-y. Xia, *Electrochem. Commun.* **2009**, *11*, 1127.
[54] C. Tran, X.-Q. Yang, D. Qu, *J. Power Sources* **2010**, *195*, 2057.
[55] C. Tran, J. Kafle, X.-Q. Yang, D. Qu, *Carbon* **2011**, *49*, 1266.
[56] P. Kichambare, J. Kumar, S. Rodrigues, B. Kumar, *J. Power Sources* **2011**, *196*, 3310.
[57] Y. Li, J. Wang, X. Li, J. Liu, D. Geng, J. Yang, R. Li, X. Sun, *Electrochem. Commun.* **2011**, *13*, 668.
[58] H. Bai, C. Li, G. Shi, *Adv. Mater.* **2011**, *23*, 1089.
[59] Q. Xiang, J. Yu, M. Jaroniec, *Chem. Soc. Rev.* **2012**, *41*, 782.
[60] Y. Si, E. T. Samulski, *Chem. Mater.* **2008**, *20*, 6792.
[61] D. R. Dreyer, S. Park, C. W. Bielawski, R. S. Ruoff, *Chem. Soc. Rev.* **2010**, *39*, 228.
[62] D. R. Dreyer, H.-P. Jia, C. W. Bielawski, *Angew. Chem. Int. Ed.* **2010**, *49*, 6813.
[63] Y. Song, K. Qu, C. Zhao, J. Ren, X. Qu, *Adv. Mater.* **2010**, *22*, 2206.
[64] Y. Li, J. Wang, X. Li, D. Geng, R. Li, X. Sun, *Chem. Commun.* **2011**, *47*, 9438.
[65] B. Sun, B. Wang, D. Su, L. Xiao, H. Ahn, G. Wang, *Carbon* **2012**, *50*, 727.
[66] R. Lakes, *Nature* **1993**, *361*, 511.
[67] J. Xiao, D. Mei, X. Li, W. Xu, D. Wang, G. L. Graff, W. D. Bennett, Z. Nie, L. V. Saraf, I. A. Aksay, J. Liu, J. G. Zhang, *Nano Lett.* **2011**, *11*, 5071.
[68] R. R. Mitchell, B. M. Gallant, C. V. Thompson, Y. Shao-Horn, *Energy Environ. Sci.* **2011**, *4*, 2952.
[69] H. Zhou, Y. Wang, H. Li, P. He, *ChemSusChem* **2010**, *3*, 1009.

[70] E. Yoo, H. Zhou, *ACS Nano* **2011**, *5*, 3020.
[71] Y. Wang, H. Zhou, *Energy Environ. Sci.* **2011**, *4*, 1704.
[72] F. Jaouen, E. Proietti, M. Lefèvre, R. Chenitz, J.-P. Dodelet, G. Wu, H. T. Chung, C. M. Johnston, P. Zelenay, *Energy Environ. Sci.* **2011**, *4*, 114.
[73] A. A. Gewirth, M. S. Thorum, *Inorg. Chem.* **2010**, *49*, 3557.
[74] S. S. Zhang, X. Ren, J. Read, *Electrochim. Acta* **2011**, *56*, 4544.
[75] X. Ren, S. S. Zhang, D. T. Tran, J. Read, *J. Mater. Chem.* **2011**, *21*, 10118.
[76] P. He, Y. Wang, H. Zhou, *Chem. Commun.* **2011**, *47*, 10701.
[77] S. Dong, X. Chen, K. Zhang, L. Gu, L. Zhang, X. Zhou, L. Li, Z. Liu, P. Han, H. Xu, J. Yao, C. Zhang, X. Zhang, C. Shang, G. Cui, L. Chen, *Chem. Commun.* **2011**, *47*, 11291.
[78] V. R. Stamenkovic, B. Fowler, B. S. Mun, G. Wang, P. N. Ross, C. A. Lucas, N. M. Markovi , *Science* **2007**, *315*, 493.
[79] J. Greeley, I. E. L. Stephens, A. S. Bondarenko, T. P. Johansson, H. A. Hansen, T. F. Jaramillo, J. Rossmeisl, I. Chorkendorff, J. K. Nørskov, *Nat. Chem.* **2009**, *1*, 552.
[80] W. Bin, *J. Power Sources* **2005**, *152*, 1.
[81] R. Bashyam, P. Zelenay, *Nature* **2006**, *443*, 63.
[82] K. Gong, F. Du, Z. Xia, M. Durstock, L. Dai, *Science* **2009**, *323*, 760.
[83] G. Wu, K. L. More, C. M. Johnston, P. Zelenay, *Science* **2011**, *332*, 443.
[84] X. Y. Yan, X. L. Tong, Y. F. Zhang, X. D. Han, Y. Y. Wang, G. Q. Jin, Y. Qin, X. Y. Guo, *Chem. Commun.* **2012**, *48*, 1892.
[85] P. Żółtowski, D. M. Dražić, L. Vorkapić, *J. Appl. Electrochem.* **1973**, *3*, 271.
[86] L. Mao, T. Sotomura, K. Nakatsu, N. Koshiba, D. Zhang, T. Ohsaka, *J. Electrochem. Soc.* **2002**, *149*, A504.
[87] L. Mao, *Electrochim. Acta* **2003**, *48*, 1015.
[88] T. Ohsaka, L. Mao, K. Arihara, T. Sotomura, *Electrochem. Commun.* **2004**, *6*, 273.
[89] F. H. B. Lima, M. L. Calegaro, E. A. Ticianelli, *J. Electroanal. Chem.* **2006**, *590*, 152.
[90] J. Yang, J. J. Xu, *Electrochem. Commun.* **2003**, *5*, 306.
[91] F. Cheng, Y. Su, J. Liang, Z. Tao, J. Chen, *Chem. Mater.* **2010**, *22*, 898.
[92] Y. L. Cao, H. X. Yang, X. P. Ai, L. F. Xiao, *J. Electroanal. Chem.* **2003**, *557*, 127.
[93] F. Cheng, J. Shen, W. Ji, Z. Tao, J. Chen, *ACS Appl. Mater. Interfaces.* **2009**, *1*, 460.
[94] N. Ominde, N. Bartlett, X.-Q. Yang, D. Qu, *J. Power Sources* **2010**, *195*, 3984.
[95] F. H. B. Lima, M. L. Calegaro, E. A. Ticianelli, *Electrochim. Acta* **2007**, *52*, 3732.
[96] J. P. Brenet, *J. Power Sources* **1979**, *4*, 183.
[97] P. Bezdička, T. Grygar, B. Klápště, J. Vondrák, *Electrochim. Acta* **1999**, *45*, 913.
[98] B. Klápště, J. Vondrák, J. Velická, *Electrochim. Acta* **2002**, *47*, 2365.
[99] I. Roche, E. Chaînet, M. Chatenet, J. Vondrák, *J. Phys. Chem. C* **2006**, *111*, 1434.
[100] I. Roche, K. Scott, *J. Appl. Electrochem.* **2008**, *39*, 197.
[101] Y. Qian, S. Lu, F. Gao, *Mater. Lett.* **2011**, *65*, 56.
[102] K. Gong, P. Yu, L. Su, S. Xiong, L. Mao, *J. Phys. Chem. C* **2007**, *111*, 1882.
[103] Z. Yang, X. Zhou, H. Nie, Z. Yao, S. Huang, *ACS Appl. Mater. Interfaces.* **2011**, *3*, 2601.
[104] J.-S. Lee, G. S. Park, H. I. Lee, S. T. Kim, R. Cao, M. Liu, J. Cho, *Nano Lett.* **2011**, *11*, 5362.
[105] J.-S. Lee, T. Lee, H.-K. Song, J. Cho, B.-S. Kim, *Energy Environ. Sci.* **2011**, *4*, 4148.
[106] Y. Gorlin, T. F. Jaramillo, *J. Am. Chem. Soc.* **2010**, *132*, 13612.
[107] M. Winter, R. J. Brodd, *Chem. Rev.* **2004**, *104*, 4245.
[108] F. Cheng, J. Shen, B. Peng, Y. Pan, Z. Tao, J. Chen, *Nat. Chem.* **2011**, *3*, 79.
[109] B. Lu, D. Cao, P. Wang, G. Wang, Y. Gao, *Int. J. Hydrogen Energy* **2011**, *36*, 72.
[110] Y. Liang, Y. Li, H. Wang, J. Zhou, J. Wang, T. Regier, H. Dai, *Nat. Mater.* **2011**, *10*, 780.
[111] J. Xu, P. Gao, T. S. Zhao, *Energy Environ. Sci.* **2012**, *5*, 5333.
[112] V. Nikolova, P. Iliev, K. Petrov, T. Vitanov, E. Zhecheva, R. Stoyanova, I. Valov, D. Stoychev, *J. Power Sources* **2008**, *185*, 727.
[113] A. Vojvodic, J. K. Nørskov, *Science* **2011**, *334*, 1355.
[114] D. Thiele, A. Züttel, *J. Power Sources* **2008**, *183*, 590.
[115] A. Hammouche, A. Kahoul, D. U. Sauer, R. W. De Doncker, *J. Power Sources* **2006**, *153*, 239.
[116] M. Yuasa, K. Shimanoe, Y. Teraoka, N. Yamazoe, *Catal. Today* **2007**, *126*, 313.
[117] J. Suntivich, H. A. Gasteiger, N. Yabuuchi, H. Nakanishi, J. B. Goodenough, Y. Shao-Horn, *Nat. Chem.* **2011**, *3*, 546.
[118] J. Suntivich, K. J. May, H. A. Gasteiger, J. B. Goodenough, Y. Shao-Horn, *Science* **2011**, *334*, 1383.
[119] M. Cheriti, A. Kahoul, *Mater. Res. Bull.* **2012**, *47*, 135.
[120] Y. Tang, B. L. Allen, D. R. Kauffman, A. Star, *J. Am. Chem. Soc.* **2009**, *131*, 13200.
[121] F. Calle-Vallejo, J. I. Martinez, J. Rossmeisl, *Phys. Chem. Chem. Phys.* **2011**, *13*, 15639.
[122] D. Geng, Y. Chen, Y. Chen, Y. Li, R. Li, X. Sun, S. Ye, S. Knights, *Energy Environ. Sci.* **2011**, *4*, 760.
[123] D. Geng, H. Liu, Y. Chen, R. Li, X. Sun, S. Ye, S. Knights, *J. Power Sources* **2011**, *196*, 1795.
[124] H. Kim, K. Lee, S. I. Woo, Y. Jung, *Phys. Chem. Chem. Phys.* **2011**, *13*, 17505.
[125] H. Li, H. Liu, Z. Jong, W. Qu, D. Geng, X. Sun, H. Wang, *Int. J. Hydrogen Energy* **2011**, *36*, 2258.
[126] S. Ni, Z. Li, J. Yang, *Nanoscale* **2012**, *4*, 1184.
[127] Y. Qiu, J. Yu, T. Shi, X. Zhou, X. Bai, J. Y. Huang, *J. Power Sources* **2011**, *196*, 9862.
[128] L. Qu, Y. Liu, J.-B. Baek, L. Dai, *ACS Nano* **2010**, *4*, 1321.
[129] W. Xiong, F. Du, Y. Liu, A. Perez, M. Supp, T. S. Ramakrishnan, L. Dai, L. Jiang, *J. Am. Chem. Soc.* **2010**, *132*, 15839.
[130] S. Wang, D. Yu, L. Dai, D. W. Chang, J.-B. Baek, *ACS Nano* **2011**, *5*, 6202.
[131] S. Shanmugam, T. Osaka, *Chem. Commun.* **2011**, *47*, 4463.
[132] S. Yang, X. Feng, X. Wang, K. Mullen, *Angew. Chem. Int. Ed.* **2011**, *50*, 5339.
[133] W. Yang, T.-P. Fellinger, M. Antonietti, *J. Am. Chem. Soc.* **2010**, *133*, 206.
[134] S. Zhu, Z. Chen, B. Li, D. Higgins, H. Wang, H. Li, Z. Chen, *Electrochim. Acta* **2011**, *56*, 5080.
[135] L. Yang, S. Jiang, Y. Zhao, L. Zhu, S. Chen, X. Wang, Q. Wu, J. Ma, Y. Ma, Z. Hu, *Angew. Chem. Int. Ed.* **2011**, *50*, 7132.
[136] S. Wang, E. Iyyamperumal, A. Roy, Y. Xue, D. Yu, L. Dai, *Angew. Chem. Int. Ed.* **2011**, *50*, 11756.
[137] K. M. Kadish, L. Frémond, J. Shen, P. Chen, K. Ohkubo, S. Fukuzumi, M. El Ojaimi, C. P. Gros, J.-M. Barbe, R. Guilard, *Inorg. Chem.* **2009**, *48*, 2571.
[138] K. M. Kadish, L. Frémond, Z. Ou, J. Shao, C. Shi, F. C. Anson, F. Burdet, C. P. Gros, J.-M. Barbe, R. Guilard, *J. Am. Chem. Soc.* **2005**, *127*, 5625.
[139] C. J. Chang, Z.-H. Loh, C. Shi, F. C. Anson, D. G. Nocera, *J. Am. Chem. Soc.* **2004**, *126*, 10013.
[140] W. Li, A. Yu, D. C. Higgins, B. G. Llanos, Z. Chen, *J. Am. Chem. Soc.* **2010**, *132*, 17056.
[141] A. Li Zhu, H. Wang, W. Qu, X. Li, Z. Jong, H. Li, *J. Power Sources* **2010**, *195*, 5587.
[142] Z. Chen, J.-Y. Choi, H. Wang, H. Li, Z. Chen, *J. Power Sources* **2011**, *196*, 3673.
[143] V. G. Khomenko, V. Z. Barsukov, A. S. Katashinskii, *Electrochim. Acta* **2005**, *50*, 1675.
[144] B. Winther-Jensen, O. Winther-Jensen, M. Forsyth, D. R. Macfarlane, *Science* **2008**, *321*, 671.